Available online at www.sciencedirect.com
SCIENCE DIRECT
Journal of Catalysis 239 (2006) 105–116
JOURNAL OF CATALYSIS
www.elsevier.com/locate/jcat

Iron-catalyzed propylene epoxidation by nitrous oxide: Toward understanding the nature of active iron sites with modified Fe-MFI and Fe-MCM-41 catalysts

Qinghong Zhang [a], Qian Guo [a], Xiaoxing Wang [a], Tetsuya Shishido [b], Ye Wang [a,*]

[a] *State Key Laboratory of Physical Chemistry of Solid Surfaces and Department of Chemistry, College of Chemistry and Chemical Engineering, Xiamen University, Xiamen 361005, China*

[b] *Department of Chemistry, Tokyo Gakugei University, Koganei, Tokyo 184-8501, Japan*

Received 2 December 2005; revised 18 January 2006; accepted 18 January 2006

Available online 10 February 2006

Abstract

Alkali metal salt (KCl)-modified Fe-MFI and Fe-MCM-41 containing iron species in different locations have been studied for the epoxidation of propylene with nitrous oxide. In the allylic oxidation of propylene without modification, the samples with iron species in the framework positions showed slightly higher activity for the formation of acrolein and allyl alcohol. After modification with KCl, propylene oxide (PO) became the main product. Significant differences in PO formation activity were observed between the samples containing iron in different locations. For the Fe-MFI and the Fe-MCM-41 prepared by the direct hydrothermal (DHT) method, in which iron was located mainly in the framework position, much lower activity was obtained after KCl modification. In contrast, the Fe-MFI after steam treatment and the Fe-MCM-41 prepared by template ion-exchange (TIE) and conventional impregnation methods, which contained extra-framework iron species (e.g., FeO_x clusters), exhibited higher PO formation activity after modification. A PO selectivity of 80% could be achieved at a propylene conversion of 3.3% over the KCl-modified Fe-MCM-41 prepared by the TIE or the impregnation method at 598 K (time on stream, 70 min). The modification with KCl increased the dispersion of the extra-framework iron species. Consequently, highly dispersed extra-framework iron species, probably in tetrahedral coordination, are proposed for the epoxidation of propylene with nitrous oxide.

Keywords: Propylene; Epoxidation; Nitrous oxide; Fe-MFI; Fe-MCM-41; Extra-framework iron

1. Introduction

Even though the silver-catalyzed epoxidation of ethylene with O_2 has been commercialized for several decades, the epoxidation of propylene remains one of the greatest challenges in catalysis [1,2]. The selectivity to propylene oxide (PO) is generally <50% in the epoxidation of propylene using O_2 as an oxidant [2–6]. The use of Ag-based catalysts with complex catalyst additives and gas-phase promoters, such as organic chloride or NO, could enhance PO formation, but PO selectivity could hardly exceed 60% even at a low propylene conversion (<5%) [2]. PO selectivity >90% was reported when H_2 was cofed with O_2 over Au–Ti- or Ag–Ti-based catalysts, where H_2O_2 generated in situ was probably responsible for the highly selective epoxidation of propylene [7–12].

In contrast, the oxidation of benzene to phenol, another challenging selective oxidation reaction, has seen significant progress thanks to the development of Fe-MFI catalyst combined with N_2O oxidant [13]. The decomposition of N_2O on active iron sites in the Fe-MFI catalyst can generate active oxygen species (known as α-oxygen) responsible for the selective oxidation of benzene to phenol [13–18]. The α-oxygen formed from N_2O on the Fe-MFI is also capable of converting CH_4 to methoxide species at room temperature, although the steady-state conversion of CH_4 with N_2O at a temperature required for N_2O decomposition could not produce CH_3OH with significant selectivity, probably due to the rapid consecutive oxidation of CH_3OH over Fe-MFI [14,19].

* Corresponding author. Fax: +86 592 2183047.
E-mail address: yewang@xmu.edu.cn (Y. Wang).

0021-9517/$ – see front matter
doi:10.1016/j.jcat.2006.01.023

The decomposition of N_2O can be expected to generate oxygen species with an electrophilic characteristic on an appropriate catalyst, which may realize the highly selective epoxidation of propylene. Thus far, only a few studies have contributed to the epoxidation of alkenes using N_2O as the oxidant. A Ru(VI) porphyrin complex and a Mn(III)-substituted polyoxometalate were used to catalyze the liquid-phase epoxidation of higher alkenes with N_2O [20,21]. For heterogeneous catalysis, two other research groups reported that modified silica gel-supported iron oxides could catalyze the epoxidation of C_3H_6 with N_2O [22,23].

In a previous paper [24], we reported the epoxidation of C_3H_6 with N_2O catalyzed by a modified FeO_x/SBA-15 catalyst. We found an interesting shift in the reaction route from allylic oxidation to epoxidation during the oxidation of C_3H_6 when the FeO_x/SBA-15 was modified by alkali metal salts, especially KCl. Recently, we clarified that over the KCl-modified FeO_x/SBA-15, KCl played the following pivotal roles in accelerating PO formation: (1) suppressing the allylic oxidation by decreasing the reactivity of lattice oxygen associated with iron species, (2) increasing the activity by raising the dispersion of iron species, and (3) eliminating the surface acidity, thereby preventing isomerization of PO [25].

Besides the roles played by alkali metal salts, the location and coordination of iron species should also be crucial for PO formation. A few reports have clarified that the local structure of iron is a key point in determining the catalytic functions of iron-containing heterogeneous catalysts. For example, for the Fe-MFI-catalyzed oxidation of benzene to phenol by N_2O, although the nature of the active species remains a matter of debate, there is a consensus that the iron species located in extra-framework positions are required for the activation of N_2O [13–18], and some recent studies have emphasized the importance of extra-framework Fe–O–Al pair sites [26–30]. The framework iron is almost inactive for this reaction. On the other hand, tetrahedral iron sites in the framework of MCM-41 have been found to be efficient for the epoxidation of styrene with H_2O_2, whereas the FeO_x clusters in the mesopores of MCM-41 are responsible only for the decomposition of H_2O_2 [31]. The tetrahedral iron site in the framework of MCM-41 is also more active and selective for partial oxidation of CH_4 to HCHO with O_2 than the extra-framework iron oxide clusters [32]. In this paper we report our recent attempts to clarify the nature of the active iron site for the epoxidation of C_3H_6 with N_2O by analyzing structure–reactivity relationships over Fe-MFI with and without steam treatment and over Fe-MCM-41 prepared by different methods.

2. Experimental

2.1. Catalyst preparation

Fe-MFI was prepared by hydrothermal synthesis following the procedure of Ratnasami and Kumar [33]. Ferric nitrate and tetraethyl orthosilicate were used as the iron and silicon sources, and tetrapropylammonium hydroxide was used as the template. The synthesis mixture was transferred to a Teflon bottle placed in a stainless steel autoclave and heated at 448 K for 120 h under stirring (70 rpm). The white solid product obtained after hydrothermal synthesis was recovered by filtration and washing with deionized water, followed by drying at 373 K and calcination at 823 K in air for 6 h. Because steam activation or high-temperature calcination is required to obtain a Fe-MFI catalyst active for the conversion of benzene to phenol by N_2O [13–18], the synthesized Fe-MFI was further treated by a steam-containing He flow (He flow rate, 30 ml min^{-1}; partial pressure of H_2O, 47 kPa) at 923 K for 8 h. The Fe-MFI after steam treatment was denoted by Fe-MFI-*s*. The samples with and without steam treatment were both further modified by KCl via the conventional impregnation method using an aqueous solution of KCl. The impregnated samples were finally calcined at 823 K for 6 h in air after drying.

Three different methods were used to prepare Fe-MCM-41. The Fe-MCM-41-DHT and Fe-MCM-41-TIE samples were prepared by the direct hydrothermal synthesis (DHT) and template ion-exchange (TIE) methods, respectively [31]. For the Fe-MCM-41-DHT sample, the iron source (ferric nitrate) was added into the synthesis gel containing the silica source (tetraethyl orthosilicate) and the template (hexadecyltrimethylammonium bromide) before hydrothermal synthesis. After hydrothermal synthesis at 393 K for 96 h, the resultant solid was filtered, washed, dried, and finally calcined at 823 K in air for 6 h. The Fe-MCM-41-TIE sample was prepared by the TIE method (i.e., exchange of the template cations embraced in the uncalcined precursor of MCM-41 with the Fe^{3+} ions in the ethanolic solution), followed by filtration, washing, drying, and calcination at 823 K. The conventional impregnation method was also applied to the preparation of iron-containing MCM-41 (denoted as Fe-MCM-41-IMP) using an ethanolic solution of [Fe(acac)$_3$] (acac = acetylacetonate). All the three types of Fe-MCM-41 were modified by KCl with the impregnation method. The powdery Fe-MCM-41 was immersed into an aqueous solution of KCl, followed by drying and calcination at 823 K.

2.2. Catalyst characterization

The iron content in each catalyst was determined by inductively coupled plasma (ICP) optical emission spectrometry (using an Agilent ICP-MS 4500-300) after the sample was dissolved with diluted nitric acid and a small amount of hydrofluoric acid. The structures of the catalysts were characterized mainly by powder X-ray diffraction (XRD), N_2-physisorption, diffuse reflectance UV–visible (UV–vis) spectroscopy, and X-ray absorption near-edge structure (XANES) spectroscopy. XRD was performed with a Panalytical X'Pert Pro Super X-ray diffractometer with Cu-K_α radiation. N_2-physisorption at 77 K was carried out with a Micromeritics TriStar 3000 surface area and porosimetry analyzer. Diffuse reflectance UV–vis spectra were recorded on a Varian Cary-5000 spectrometer equipped with a diffuse-reflectance accessory. The spectra were collected at 200–800 nm with $BaSO_4$ as a reference. XANES measurements were carried out for some typical samples with synchrotron radiation in the High-Energy Accelerator Research Or-

ganization (Tsukuba, Japan). The data were recorded in X-ray fluorescence mode at room temperature using a Si(111) double-crystal monochromator. Energy was calibrated with Cu K-edge absorption (8981.0 eV), with an energy resolution of 0.3 eV. The absorption was normalized to 1.0 at an energy position 30 eV higher than the absorption edge.

2.3. Catalytic reaction

The catalytic reactions were carried out using a fixed-bed flow reactor operated at atmospheric pressure. Typically, 0.20 g of catalyst was pretreated in the quartz reactor (10 mm i.d.) with a gas flow containing high-purity He (99.99%, 40 $cm^3\,min^{-1}$) and O_2 (99.99%, 10 $cm^3\,min^{-1}$) at 823 K for 1 h, followed by purging with the high-purity He (60 $cm^3\,min^{-1}$) at the same temperature for 1 h before reaction. Then the reactant gas flow containing C_3H_6 (99.9%) and N_2O (>99.9%) diluted with He (99.99%) was introduced into the reactor to start the reaction after the catalyst bed had reached the desired reaction temperature (typically 598 K). The products were analyzed by on-line gas chromatography. All the lines and valves between the exit of the reactor and the gas chromatographs were heated to 393 K to prevent condensation of the products. PO, acrolein, allyl alcohol, acetone, acetaldehyde, and other oxygenated products were separated by a Porapak T column and were detected by a flame ionization detector. The separation and detection of other components, such as O_2, N_2, N_2O, C_3H_6, CO, and CO_2 were carried out by Porapak Q and Molecular Sieve 5A columns and thermal conductivity detectors. C_3H_6 conversions were evaluated from the concentrations of the products detected (i.e., PO, acrolein, allyl alcohol, acetone, propionaldehyde, acetaldehyde, CO, and CO_2) and the remaining C_3H_6. Similar to the modified FeO_x/SBA-15 catalyst reported previously [24], deactivation of Fe-MFI and the Fe-MCM-41 series of catalysts was also observed with time on stream. The results after 70 min of reaction were typically shown and used for discussion, unless otherwise stated.

3. Results

3.1. Catalytic behaviors of the Fe-MFI-related catalysts

Table 1 shows the catalytic properties of the Fe-MFI (Si/Fe = 64)-related samples for the oxidation of C_3H_6 with N_2O. Pure siliceous MFI zeolite without iron did not show C_3H_6 conversion activity before or after the addition of KCl under our reaction conditions, strongly suggesting that the iron species were responsible for the oxidation of C_3H_6. The Fe-MFI mainly catalyzed the allylic oxidation of C_3H_6 by N_2O, giving acrolein and allyl alcohol with selectivities of 57 and 14%, respectively. PO was also formed, but with only low selectivity (3.0%). The direct modification of Fe-MFI with KCl shifted the main reaction route from allylic oxidation to epoxidation, with PO selectivity increasing to 48 and 57% at K/Fe molar ratios of 1 and 2, respectively. A selectivity shift was also observed for FeO_x/SBA-15 [24,25]. However, in contrast to the observation that C_3H_6 conversion increased after the addition of KCl for FeO_x/SBA-15, the direct modification of the Fe-MFI with KCl significantly decreased the C_3H_6 conversion from 1.2 to 0.15% (with K/Fe = 1) or to 0.29% (with K/Fe = 2).

Compared with Fe-MFI without steam treatment, steam-treated Fe-MFI (Fe-MFI-*s*) before KCl modification showed a lower C_3H_6 conversion but no significant change in the sum of the selectivities to acrolein and allyl alcohol. However, modification of Fe-MFI-*s* with KCl not only caused the formation of PO as a main product, but also increased C_3H_6 conversion. Thus, after modification with KCl, Fe-MFI-*s* exhibited significantly higher activity for PO formation than Fe-MFI without steam treatment. As shown in Table 1, the turnover frequency (TOF) values for PO formation over the KCl–Fe-MFI-*s* with K/Fe molar ratios of 1 and 2 were more than 6 and 3 times higher than those over the corresponding KCl–Fe-MFI, respectively.

Table 1
Catalytic properties of Fe-MFI-related catalysts for the oxidation of C_3H_6 with N_2O[a]

Catalyst	C_3H_6 conversion (%)	Selectivity (%)					TOF[c] (h^{-1})
		PO	Acrolein	Allyl alcohol	Others[b]	CO_x	
Silicate (MFI)	0	–	–	–	–	–	0
KCl-silicate (MFI)[d]	0	–	–	–	–	–	0
Fe-MFI (Si/Fe = 64)	1.2	3.0	57	14	0	26	0.029
KCl–Fe-MFI[e]	0.15	48	7.0	2.5	15	28	0.058
KCl–Fe-MFI[f]	0.29	57	4.2	2.8	10	26	0.14
Fe–MFI-*s* (Si/Fe = 64)	0.75	0.3	62	10	9.7	18	0.018
KCl–Fe-MFI-*s*[e]	1.1	46	6.0	2.0	18	28	0.40
KCl–Fe-MFI-*s*[f]	0.89	64	4.0	1.7	8.3	22	0.46
KCl–Fe-MFI-*s*[g]	0.81	60	3.6	2.8	7.6	26	0.41

[a] Reaction conditions: catalyst, 0.2 g; total flow rate, 60 ml min^{-1}; $P(C_3H_6) = 2.5$ kPa; $P(N_2O) = 25.3$ kPa; $T = 598$ K.
[b] Other products mainly included acetone and acetaldehyde.
[c] TOF was evaluated from the moles of PO formed per hour per mole of Fe in the catalyst.
[d] K/Si = 0.04.
[e] K/Fe = 1.0.
[f] K/Fe = 2.0.
[g] K/Fe = 4.0.

Table 2
Catalytic properties of different series of Fe-MCM-41 prepared by different methods for the oxidation of C_3H_6 with N_2O[a]

Catalyst	Si/Fe	C_3H_6 conversion (%)	Selectivity (%)					TOF[c] (h^{-1})
			PO	Acrolein	Allyl alcohol	Others[b]	CO_x	
MCM-41	∞	0						0
Fe-MCM-41-DHT	189	1.4	0.2	54	13	7.4	25	0.0062
Fe-MCM-41-DHT	141	1.5	0.4	54	12	8.2	25	0.011
Fe-MCM-41-DHT	110	1.8	0	50	4.2	8.8	37	0
Fe-MCM-41-TIE	207	0.80	0.3	62	8.2	7.0	22	0.0060
Fe-MCM-41-TIE	168	1.1	0.3	58	11	7.0	24	0.0065
Fe-MCM-41-TIE	123	1.3	2.0	55	2.6	6.9	34	0.038
Fe-MCM-41-IMP	200	0.90	0.3	58	10	7.0	25	0.0077
Fe-MCM-41-IMP	150	1.1	0.8	56	18	7.4	16	0.016
Fe-MCM-41-IMP	92	1.1	0.7	52	11	7.7	29	0.0082
α-Fe_2O_3	0	0.34	0	11	0	1.0	88	0

[a] Reaction conditions: catalyst, 0.2 g; total flow rate, 60 ml min^{-1}; $P(C_3H_6) = 2.5$ kPa; $P(N_2O) = 25.3$ kPa; $T = 598$ K.
[b] Other products mainly included acetone and acetaldehyde.
[c] TOF was evaluated from the moles of PO formed per hour per mole of Fe in the catalyst.

Table 3
Catalytic properties of different series of Fe-MCM-41 after modification of KCl for the oxidation of C_3H_6 with N_2O[a]

Catalyst[b]	Si/Fe	C_3H_6 conversion (%)	Selectivity (%)					TOF[d] (h^{-1})
			PO	Acrolein	Allyl alcohol	Others[c]	CO_x	
KCl-MCM-41[e]	∞	0	–	–	–	–	–	0
KCl–Fe-MCM-41-DHT	189	0.09	80	6.2	0.1	9.0	4.7	0.17
KCl–Fe-MCM-41-DHT	141	0.15	81	3.2	4.3	5.0	5.2	0.21
KCl–Fe-MCM-41-DHT	110	0.31	80	3.8	4.2	4.9	7.5	0.33
KCl–Fe-MCM-41-TIE	207	2.0	83	2.4	2.1	5.3	7.4	4.3
KCl–Fe-MCM-41-TIE	168	3.3	79	3.0	2.4	6.7	8.5	5.4
KCl–Fe-MCM-41-TIE	123	4.0	67	3.8	1.9	11	16	4.1
KCl–Fe-MCM-41-IMP	200	2.0	85	2.4	2.2	4.2	6.1	4.1
KCl–Fe-MCM-41-IMP	150	3.3	80	2.9	2.9	6.7	7.7	4.9
KCl–Fe-MCM-41-IMP	92	3.7	73	1.1	1.1	7.7	17	3.1
KCl−α-Fe_2O_3	0	0	–	–	–	–	–	0

[a] Reaction conditions: catalyst, 0.2 g; total flow rate, 60 ml min^{-1}; $P(C_3H_6) = 2.5$ kPa; $P(N_2O) = 25.3$ kPa; $T = 598$ K.
[b] Molar ratio of K/Fe in each catalyst containing Fe was 2/1.
[c] Other products mainly included acetone and acetaldehyde.
[d] TOF was evaluated from the moles of PO formed per hour per mole of Fe in the catalyst.
[e] K/Si = 0.04.

3.2. Catalytic behaviors of the Fe-MCM-41-related catalysts

Table 2 shows the catalytic results of the Fe-MCM-41 samples prepared by different methods for the oxidation of C_3H_6 with N_2O. All of these samples gave acrolein as the main product, with no PO or only a minor amount of PO (TOF for PO formation <0.04 h^{-1}). MCM-41 was inactive for the oxidation of C_3H_6 under our conditions, and α-Fe_2O_3 showed both lower C_3H_6 conversion and lower acrolein selectivity. For each series of samples, C_3H_6 conversion increased slightly with increasing iron content (decreasing Si/Fe ratio), and the selectivity to acrolein decreased slightly. The comparisons among different series of samples with similar iron contents showed that C_3H_6 conversions over the Fe-MCM-41-DHT series of samples were higher than those over the Fe-MCM-41-TIE and Fe-MCM-41-IMP series of samples, and that the latter two series of samples exhibited similar activities.

After modification with KCl, PO became the main product over all three series of catalysts, as shown in Table 3. PO selectivity exceeded 80% in some cases. However, the three series exhibited significant differences in C_3H_6 conversion. For the Fe-MCM-41-DHT series, C_3H_6 conversion dropped significantly, to $<0.35\%$, after KCl modification. In contrast, KCl modification of the Fe-MCM-41-TIE and Fe-MCM-41-IMP series (K/Fe = 2) significantly (2- to 3-fold) enhanced the conversion of C_3H_6. Compared with the modified Fe-MCM-41-DHT catalyst, the TOF values for PO formation were >10 times higher for the KCl-modified Fe-MCM-41-TIE and Fe-MCM-41-IMP catalysts. The TOF values obtained over these latter two catalysts were also significantly greater than those obtained over KCl-modified Fe-MFI catalysts with or without steam treatment.

The effects of K/Fe molar ratio on the conversion of C_3H_6 and the TOF for PO formation over the three series of catalysts with comparable iron content are shown in Fig. 1. The results for the Fe-MCM-41-DHT (Si/Fe = 110) series of samples showed that the addition of KCl with a K/Fe ratio of 1.0 already greatly decreased C_3H_6 conversion, and a further increase in K/Fe ratio had no significant affect on C_3H_6 conversion. An increase in the K/Fe ratio from 0 to 4.0 raised the TOF for PO

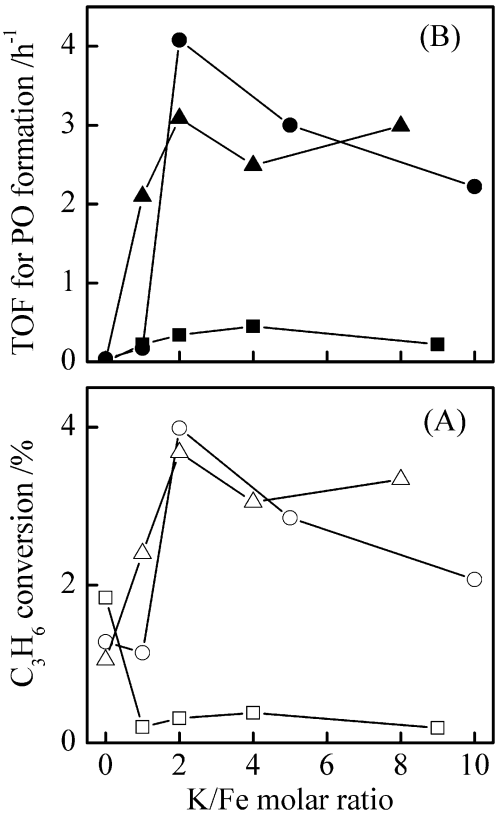

Fig. 1. Effect of K/Fe molar ratio on catalytic behaviors for the Fe-MCM-41 samples prepared by different methods. Reaction conditions: catalyst, 0.2 g; total flow rate, 60 ml min^{-1}; $P(C_3H_6)$ = 2.5 kPa; $P(N_2O)$ = 25.3 kPa; T = 598 K. (A) C_3H_6 conversion: (□) Fe-MCM-41-DHT (Si/Fe = 110), (○) Fe-MCM-41-TIE (Si/Fe = 123), (△) Fe-MCM-41-IMP (Si/Fe = 92); (B) TOF for PO formation: (■) Fe-MCM-41-DHT (Si/Fe = 110), (●) Fe-MCM-41-TIE (Si/Fe = 123), (▲) Fe-MCM-41-IMP (Si/Fe = 92).

formation slightly, but the maximum TOF was only 0.45 h^{-1}. In contrast, for the Fe-MCM-41-TIE and Fe-MCM-41-IMP series of samples, both the conversion of C_3H_6 and the TOF for PO formation increased significantly with an increase in the K/Fe ratio from 0 to 2.0. The TOF values obtained over the KCl-modified Fe-MCM-41-TIE and Fe-MCM-41-IMP samples with a K/Fe ratio of 2.0 were 4.1 and 3.1 h^{-1}, respectively. Further increases in the K/Fe ratio decreased the conversion of C_3H_6 and the TOF for PO formation for the Fe-MCM-41-TIE series, but had no significant affect on the Fe-MCM-41-IMP series.

The changes in catalytic performance with time on stream over the KCl-modified Fe-MCM-41-DHT (Si/Fe = 110), Fe-MCM-41-TIE (Si/Fe = 123), and Fe-MCM-41-IMP (Si/Fe = 92) samples with a K/Fe ratio of 2.0 are shown in Fig. 2. The KCl–Fe-MCM-41-DHT sample exhibited very low C_3H_6 conversion at all times on stream investigated. C_3H_6 conversion over the KCl–Fe-MCM-41-TIE and the KCl–Fe-MCM-41-IMP samples decreased with time on stream, but PO selectivity either did not change significantly or increased only slightly. These tendencies were similar to those observed for the epoxidation of C_3H_6 by an O_2–H_2 gas mixture over Au/Ti-based catalysts [10]. We have clarified that carbon deposition is a main reason for the catalyst deactivation in our case, and the activity

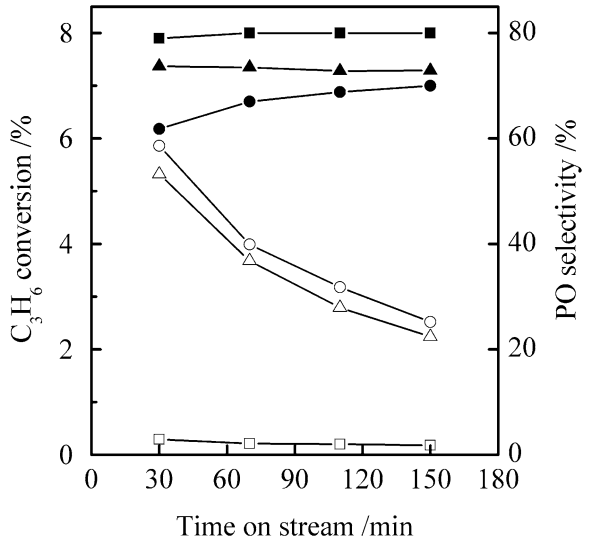

Fig. 2. Changes of catalytic performances with time on stream for the KCl-modified Fe-MCM-41 samples prepared by different methods (K/Fe= 2.0). Reaction conditions: catalyst, 0.2 g; total flow rate, 60 ml min^{-1}; $P(C_3H_6)$ = 2.5 kPa; $P(N_2O)$ = 25.3 kPa; T = 598 K. C_3H_6 conversion: (□) KCl–Fe-MCM-41-DHT, (○) KCl–Fe-MCM-41-TIE, (△) KCl–Fe-MCM-41-IMP; PO selectivity: (■) KCl–Fe-MCM-41-DHT, (●) KCl–Fe-MCM-41-TIE, (▲) KCl–Fe-MCM-41-IMP.

can be recovered almost completely by regenerating the catalyst with a gas flow containing He and O_2 at 823 K for 30 min.

3.3. Structure features of the Fe-MFI-related catalysts

Fig. 3 shows the XRD patterns for the Fe-MFI, Fe-MFI-*s*, and KCl-modified Fe-MFI and Fe-MFI-*s* samples. The Fe-MFI (Si/Fe = 64) synthesized in this work exhibited the characteristic XRD pattern of the MFI structure (curve a). No XRD peaks ascribed to α-Fe_2O_3 were observed. Steam treatment of the Fe-MFI did not significantly change the XRD pattern of the MFI structure (curve d). Thus the steam treatment at 923 K did not cause a collapse of the zeolite structure or the appearance of crystalline α-Fe_2O_3. Moreover, the MFI structure was also maintained after modification of both the Fe-MFI and the Fe-MFI-*s* samples with KCl. For the samples with a K/Fe molar ratio of 1 (KCl content, 1.9 wt%), the peaks of crystalline KCl were not observed, possibly because of the high dispersion of KCl or the low KCl content (curves b and e). However, as the K/Fe ratio increased to 2 (KCl, 3.7 wt%), XRD peaks at 28.3° and 40.5° (2θ degrees) assigned to crystalline KCl became clear for both KCl–Fe-MFI and the KCl–Fe-MFI-*s* (curves c and f), suggesting the segregation of crystalline KCl particles at higher K/Fe ratios. No other phases were formed even after the addition of KCl with a K/Fe ratio of 4 to the Fe-MFI-*s* (curve g).

The white color of the Fe-MFI was not altered after the direct modification with KCl. The change in color to brown was observed after steam treatment at 873 K, and it was of interest that the modification of the brown Fe-MFI-*s* with KCl returned the color to white again (Table 4). This strongly suggests variations in the structure of iron during the steam treatment and the further KCl modification. We have clarified that diffuse reflectance UV–vis spectroscopic studies can clearly follow such changes.

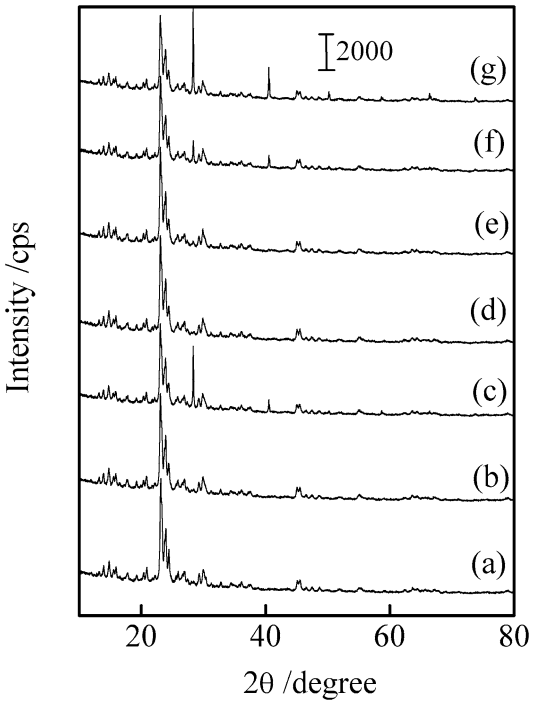

Fig. 3. XRD patterns: (a) Fe-MFI (Si/Fe = 64), (b) KCl–Fe-MFI (K/Fe = 1), (c) KCl–Fe-MFI (K/Fe = 2), (d) Fe-MFI-*s* (Si/Fe = 64), (e) KCl–Fe-MFI-*s* (K/Fe = 1), (f) KCl–Fe-MFI-*s* (K/Fe = 2), (g) KCl–Fe-MFI-*s* (K/Fe = 4).

Table 4
Colors, band gap energy (E_g) values for Fe–O band, and Fe K-edge XANES pre-edge peak areas of the Fe-MFI series of samples together with α-Fe_2O_3

Sample	Color	E_g (eV)	XANES pre-edge peak area[a]
α-Fe_2O_3	Reddish brown	2.10	6.1
Fe-MFI (Si/Fe = 64)	White	4.68	24.1
KCl–Fe-MFI (K/Fe = 1)	White	4.71	n.d.
Fe-MFI-*s* (Si/Fe = 64)	Brown	3.18	18.9
KCl–Fe-MFI-*s* (K/Fe = 1)	White	4.65	n.d.
KCl–Fe-MFI-*s* (K/Fe = 2)	White	4.65	24.2
KCl–Fe-MFI-*s* (K/Fe = 4)	White	4.64	n.d.
4-coordinated iron complex[b]	–	–	23.1–25.0
5-coordinated iron complex[b]	–	–	12.4–18.8
6-coordinated iron complex[b]	–	–	5.8–9.3

[a] Normalized area expressed in 10^{-2} eV units.
[b] From Ref. [42].

As shown in Fig. 4, the Fe-MFI sample exhibited absorption bands at 218 and 238 nm (overlapped) in the UV–vis spectrum (curve a). Bordiga et al. [34] reported that the tetrahedral Fe^{3+} sites isomorphously incorporated into the framework of MFI zeolite exhibited two UV absorption bands at 215 and 241 nm, very close to our observation. These two bands may correspond to $t_1 \rightarrow t_2$ and $t_1 \rightarrow e$ transitions for the Fe^{3+} (d^5) in the tetrahedral coordination with oxygen, where the high-spin $e^2t_2^3$ configuration is favored over the $e^4t_2^1$ configuration because the crystal field is not strong enough to cause spin-pairing [34,35]. Direct modification of the Fe-MFI sample with KCl did not significantly change the UV–vis spectrum (curve b); however, after the Fe-MFI sample was treated with steam at 923 K, a distinct broad shoulder at >300 nm appeared, and the absorption edge

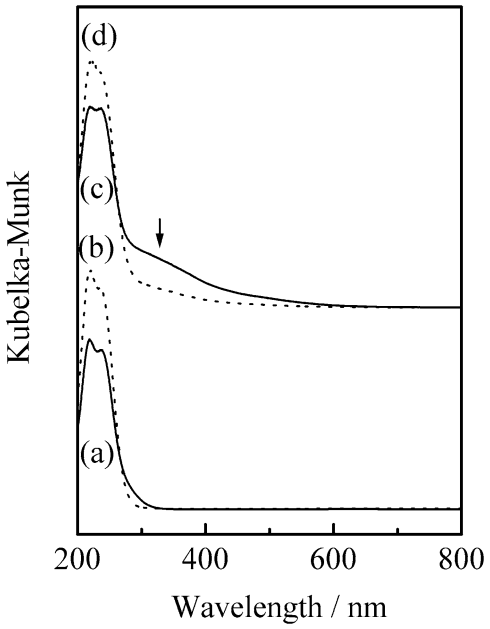

Fig. 4. Diffuse reflectance UV–vis spectra: (a) Fe-MFI (Si/Fe = 64), (b) KCl–Fe-MFI (K/Fe = 1), (c) Fe-MFI-*s* (Si/Fe = 64), (d) KCl–Fe-MFI-*s* (K/Fe = 1).

shifted to a significantly longer wavelength position (curve c). Further modification of the Fe-MFI-*s* sample with KCl shifted the absorption edge back to the UV region (curve d).

It is well known that for the transition metal oxide species, the energy of the absorption edge corresponds to the band gap energy (E_g), and the E_g generally changes with the dispersion and the local coordination structure of the species [36]. The correlations between the E_g values and the local structures around Mo^{6+} and V^{5+} were analyzed by Weber [36] and Gao and Wachs [37], respectively, who showed convincingly that the E_g value can be used to determine the local structures of Mo and V. For the supported MoO_x or VO_x samples, the E_g value generally decreases in the following sequence: tetrahedral VO_4 or MoO_4 monomer > octahedral VO_6 or MoO_6 oligomer > octahedral VO_6 or MoO_6 polymer [36,37]. Iwamoto et al. [38] observed a significant increase in E_g value from 2.14 eV for the bulk α-Fe_2O_3 to 4.20 eV for iron oxide nanoclusters introduced into the mesoporous channels of MCM-41. However, to the best of our knowledge, using the E_g value to identify the local coordination of iron has not been reported before the present study. We have evaluated the E_g value for the Fe–O band from the UV–vis spectra for each sample using the method proposed by Weber [36], that is, finding the energy intercept of the straight line in the plot of $[F(R_\infty) \times h\nu]^2$ versus $h\nu$, where $F(R_\infty)$ is the Kubelka–Munk function and $h\nu$ is the incident photo energy. As shown in Table 4, the decrease in E_g observed after steam treatment corresponded closely to the transformation of the tetrahedral iron sites isolated in the framework into oligomeric FeO_x species in the extra-framework positions. This is consistent with the expectation that the tetrahedral iron would be extracted from the framework positions by hydrolysis of the Si–O–Fe bonds, possibly forming oligonuclear FeO_x species or iron oxide nanoparticles in the extra-framework positions [18,

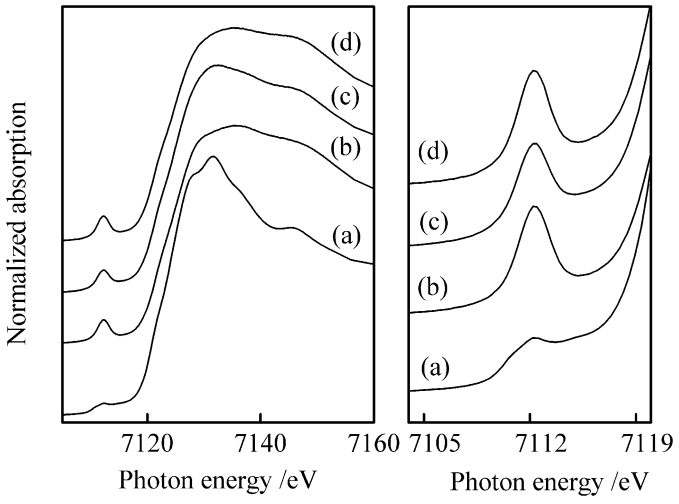

Fig. 5. Fe K-edge XANES spectra: (a) α-Fe_2O_3, (b) Fe-MFI (Si/Fe = 64), (c) Fe-MFI-*s* (Si/Fe = 64), (d) KCl–Fe-MFI-*s* (K/Fe = 1).

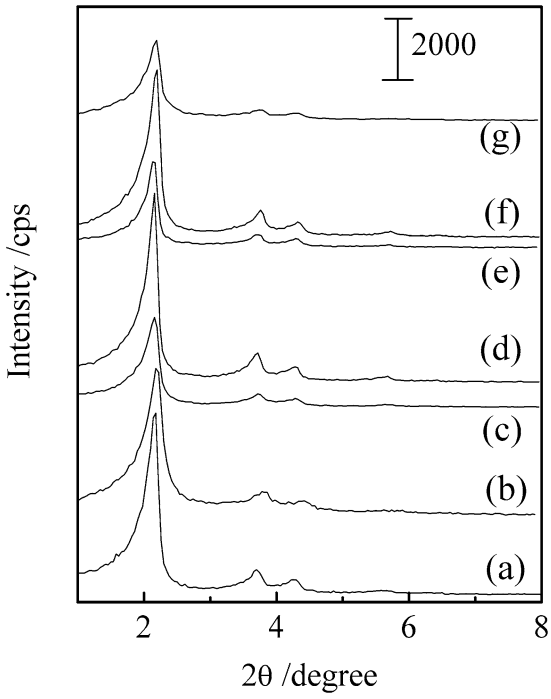

Fig. 6. XRD patterns at low diffraction angles for MCM-41 and Fe-MCM-41: (a) MCM-41, (b) Fe-MCM-41-DHT (Si/Fe = 189), (c) Fe-MCM-41-DHT (Si/Fe = 110), (d) Fe-MCM-41-TIE (Si/Fe = 207), (e) Fe-MCM-41-TIE (Si/Fe = 123), (f) Fe-MCM-41-IMP (Si/Fe = 200), (g) Fe-MCM-41-IMP (Si/Fe = 92).

39–41]. We did not observe the crystalline iron oxide peaks in the XRD pattern (Fig. 3) probably because the FeO_x particles were very small or the iron content in the catalyst was too low (<2 wt%). KCl modification of the steam-treated sample increased the E_g value to close to that for the Fe-MFI sample, indicating that dispersion of the extra-framework iron species in the Fe-MFI-*s* sample was enhanced through the interaction with KCl.

We carried out XANES studies to further elucidate the changes in the local coordination of iron. Fig. 5 shows the Fe K-edge XANES spectra for the Fe-MFI, Fe-MFI-*s*, and KCl–Fe-MFI-*s* samples, as well as for α-Fe_2O_3. The Fe-MFI sample exhibited a distinct pre-edge peak assigned to the 1s–3d transition at ca. 7112 eV; the pre-edge peak for α-Fe_2O_3 was much weaker. It is known that the intensity (I) of the pre-edge peak is determined by the local coordination of iron and decreases in the following sequence: I(tetrahedral) > I(square pyramidal) > I(octahedral) [25,42]. The pre-edge peak areas evaluated from Fig. 5 are listed in Table 4. The data for iron complexes with four, five, and six coordinations reported by Roe et al. [42] are also listed in the table for comparison. After steam treatment of the Fe-MFI sample, a slight decrease in the intensity of the pre-edge peak and a change in the oscillation by XANES at the high-energy region were observed, suggesting a change in the coordination of iron. After KCl modification of the Fe-MFI-*s* sample, the pre-edge peak area increased again, and the XANES pattern also recovered to where it was almost the same with that for the Fe-MFI sample. Therefore, it is reasonable to consider that the coordination of iron was transformed into a tetrahedral configuration in the KCl–Fe-MFI-*s* sample.

3.4. Structure characteristics of the Fe-MCM-41-related catalysts

XRD measurements at low diffraction angles ($2\theta = 1°$–$8°$) were carried out to obtain information about the regularity of mesoporous structures. As shown in Fig. 6, before KCl modification, all three series of samples exhibited three diffraction peaks at 2θ degrees of ca. 2.2°, 3.8°, and 4.3° ascribed to (100), (110), and (200) of the hexagonal regularity of mesoporous structure of MCM-41. Thus the ordered hexagonal array of mesopores was sustained after the introduction of iron species into MCM-41 by all three methods. After KCl modification, the three peaks were still clearly observed for the Fe-MCM-41-TIE and the Fe-MCM-41-IMP series of samples (Fig. 7, curves c–f), indicating maintenance of the long-range regularity of the mesoporous structure for these modified samples. However, for the KCl-modified Fe-MCM-41-DHT samples, the mesoporous structure collapsed. Only the peak of (100) was observable for the KCl–Fe-MCM-41-DHT sample with a Si/Fe ratio of 189 (K/Fe = 2), and no peak could be discerned at the low diffraction angles for the KCl–Fe-MCM-41-DHT sample with a Si/Fe ratio of 110 (K/Fe = 2).

The parameters concerning mesoporous structures derived from N_2-sorption measurements are shown in Table 5. For the Fe-MCM-41-TIE and the Fe-MCM-41-IMP series of samples, the BET surface area and pore volume decreased gradually with the addition of KCl. Pore diameter, evaluated by the BJH method, also decreased at the same time. These decreases might suggest that the mesopores of MCM-41 were filled with KCl species. On the other hand, the surface area and the pore volume decreased significantly after the addition of KCl with a K/Fe ratio of 1 to the Fe-MCM-41-DHT sample. This is consistent with the XRD results shown in Fig. 7 (curves a and b), indicating that the ordered mesoporous structure of the Fe-MCM-41-DHT was destroyed by KCl. We believe that the collapse of the ordered

Table 5
Physical parameters for three series of Fe-MCM-41 samples before and after KCl modification derived from N_2 sorption and UV–vis spectroscopic measurements

Sample	Si/Fe	S_{BET} ($m^2\ g^{-1}$)	Pore volume ($cm^3\ g^{-1}$)	Pore diameter (nm)	Color	E_g (eV)
MCM-41	–	950	0.90	2.9	White	–
Fe-MCM-41-DHT	110	1006	0.91	3.0	White	4.50
KCl–Fe-MCM-41-DHT[a]	110	158	0.24	3.5	Brown	2.80
KCl–Fe-MCM-41-DHT[b]	110	138	0.21	3.5	Brown	2.75
Fe-MCM-41-TIE	123	906	0.73	2.8	Pale brown	4.03
KCl–Fe-MCM-41-TIE[a]	123	564	0.53	2.6	White	4.53
KCl–Fe-MCM-41-TIE[b]	123	488	0.39	2.5	White	4.59
Fe-MCM-41-IMP	92	860	0.72	2.8	Pale brown	4.05
KCl–Fe-MCM-41-IMP[a]	92	610	0.51	2.7	White	4.54
KCl–Fe-MCM-41-IMP[b]	92	418	0.31	2.5	White	4.58

[a] K/Fe = 1.
[b] K/Fe = 2.

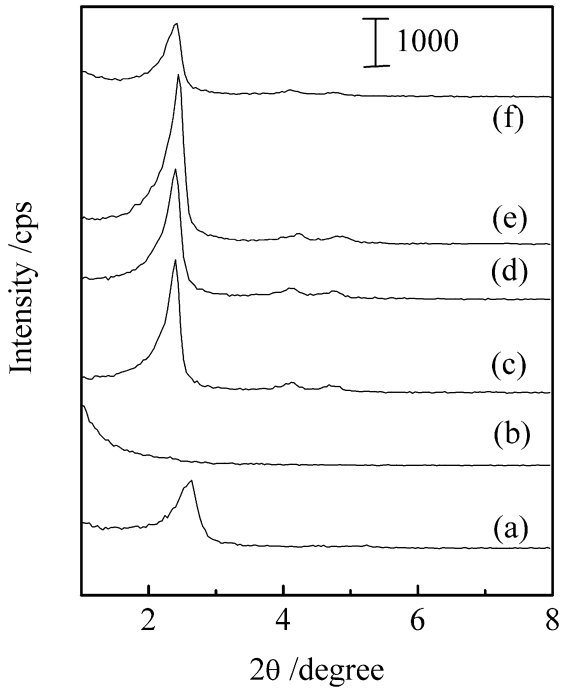

Fig. 7. XRD patterns at low diffraction angles for KCl–Fe-MCM-41 (K/Fe = 2): (a) KCl–Fe-MCM-41-DHT (Si/Fe = 189), (b) KCl–Fe-MCM-41-DHT (Si/Fe = 110), (c) KCl–Fe-MCM-41-TIE (Si/Fe = 207), (d) KCl–Fe-MCM-41-TIE (Si/Fe = 123), (e) KCl–Fe-MCM-41-IMP (Si/Fe = 200), (f) KCl–Fe-MCM-41-IMP (Si/Fe = 92).

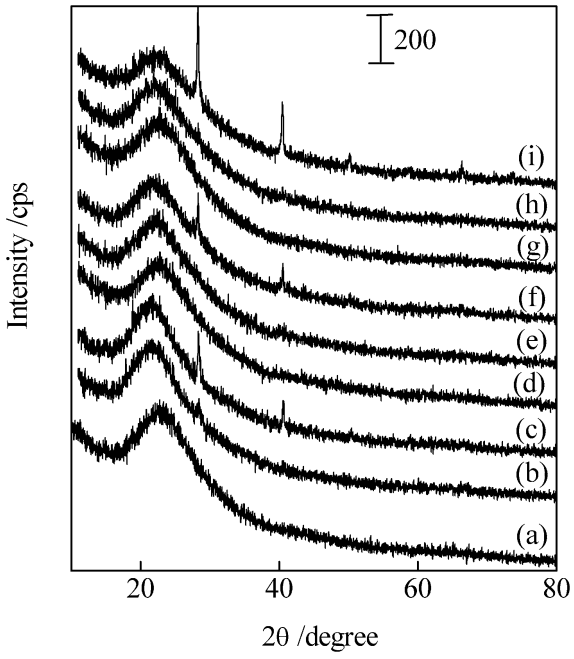

Fig. 8. XRD patterns at high diffraction angles for Fe-MCM-41 and KCl–Fe-MCM-41: (a) Fe-MCM-41-DHT (Si/Fe = 110), (b) KCl–Fe-MCM-41-DHT (Si/Fe = 110, K/Fe = 2), (c) KCl–Fe-MCM-41-DHT (Si/Fe = 110, K/Fe = 4), (d) Fe-MCM-41-TIE (Si/Fe = 123), (e) KCl–Fe-MCM-41-TIE (Si/Fe = 123, K/Fe = 5), (f) KCl–Fe-MCM-41-TIE (Si/Fe = 123, K/Fe = 10), (g) Fe-MCM-41-IMP (Si/Fe = 92), (h) KCl–Fe-MCM-41-IMP (Si/Fe = 92, K/Fe = 4), (i) KCl–Fe-MCM-41-IMP (Si/Fe = 92, K/Fe = 8).

hexagonal structure may have resulted from the strong interaction of KCl with the Fe-MCM-41-DHT sample.

Fig. 8 shows the XRD patterns at high diffraction angles ($2\theta = 10°$–$80°$) for the three series of Fe-MCM-41 samples with and without modification. Without modification, all of the Fe-MCM-41 samples exhibited a broad peak at only ca. 22°, assigned to the amorphous feature of the framework of MCM-41. No information about the structure of iron species can be inferred from the XRD findings because of the samples' low iron content. For the KCl–Fe-MCM-41-DHT series, a weak peak at 28.5° assignable to crystalline KCl already appeared at a K/Fe ratio of 2.0 (KCl content, 2.2 wt%) (curve b). In contrast, a peak of KCl was not observed over the KCl–Fe-MCM-41-TIE and the KCl–Fe-MCM-41-IMP series even with higher KCl content. For example, no crystalline KCl was observed at a K/Fe ratio of 5 (KCl content, 4.8 wt%) for the KCl–Fe-MCM-41-TIE sample (curve e) or at a K/Fe ratio of 4 (KCl content, 5.1 wt%) for the KCl–Fe-MCM-41-IMP (curve h). For these two series of samples, crystalline KCl was observed only at much higher K/Fe ratios (e.g., K/Fe = 10 for Fe-MCM-41-TIE and 8 for Fe-MCM-41-IMP). Therefore, KCl was more highly dispersed over these two series of samples. Considering these findings along with the XRD at low diffraction angles and the N_2-sorption results, we speculate that KCl was located mostly inside the mesopores in the KCl–Fe-MCM-41-TIE and

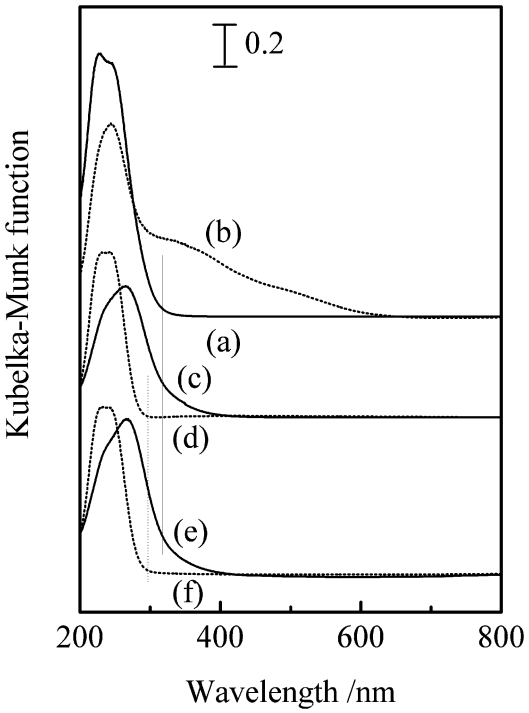

Fig. 9. Diffuse reflectance UV–vis spectra: (a) Fe-MCM-41-DHT (Si/Fe = 110), (b) KCl–Fe-MCM-41-DHT (Si/Fe = 110, K/Fe = 2), (c) Fe-MCM-41-TIE (Si/Fe = 123), (d) KCl–Fe-MCM-41-TIE (Si/Fe = 123, K/Fe = 2), (e) Fe-MCM-41-IMP (Si/Fe = 92), (f) KCl–Fe-MCM-41-IMP (Si/Fe = 92, K/Fe = 2).

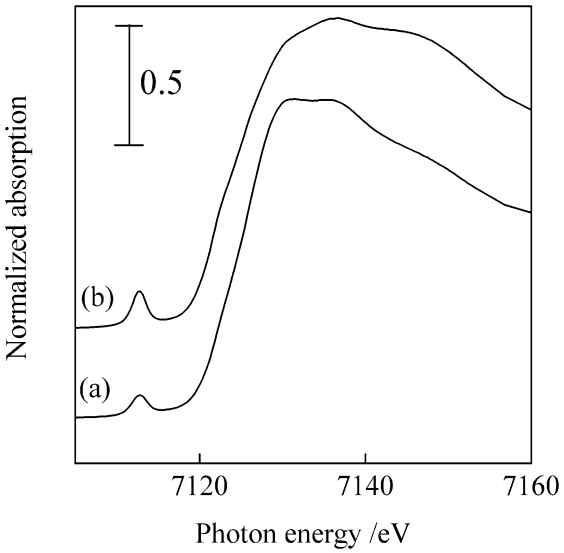

Fig. 10. Fe K-edge XANES spectra: (a) Fe-MCM-41-TIE (Si/Fe = 123), (b) KCl–Fe-MCM-41-TIE (Si/Fe = 123, K/Fe = 2).

the KCl–Fe-MCM-41-IMP series of samples with K/Fe ratios <5 and 4, respectively. On the other hand, because the mesoporous structure of the Fe-MCM-41-DHT was destroyed after the addition of KCl, the crystalline KCl segregated even at a relatively lower K/Fe ratio.

The structures of iron in the three series of Fe-MCM-41 with and without KCl modification were investigated by diffuse reflectance UV–vis spectroscopy. As shown in Fig. 9, the UV–vis spectra of the Fe-MCM-41-TIE and Fe-MCM-41-IMP samples resembled each other (curves c and e) and exhibited relatively broad absorption bands at ca. 265 nm. These bands could be ascribed to the ligand (O^{2-})–metal (Fe^{3+}) charge transfer (LMCT) transition. After modification with KCl, the LMCT transitions in both cases apparently shifted to shorter-wavelength positions (curves d and f). This tendency was the same as that observed for FeO_x/SBA-15 after KCl modification [25]. In contrast, although the Fe-MCM-41-DHT sample without modification exhibited a double set of peaks at short-wavelength positions (curve a) resembling that observed for the Fe-MFI sample (Fig. 4), distinct absorptions were observed at longer wavelengths (extending to ca. 620 nm) after the addition of KCl (curve b of Fig. 9).

The E_g values calculated from the UV–vis spectra are summarized in Table 5. The Fe-MCM-41-DHT, Fe-MCM-41-TIE, and Fe-MCM-41-IMP samples had E_g values of 4.50, 4.03, and 4.05 eV, respectively, indicating that the dispersion of iron was greater in the first sample than in the latter two samples. In previous work [31], we clarified, through XANES and EXAFS measurements, that iron cations in the Fe-MCM-41-DHT sample with iron content < ca. 1 wt% (Si/Fe ≈ 100) were located mainly in the tetrahedral framework positions of MCM-41, whereas small FeO_x clusters with iron in octahedral coordination existed mainly in the Fe-MCM-41-TIE sample. The E_g values obtained here for the two samples are in good agreement with this conclusion. Moreover, we can infer that the Fe-MCM-41-IMP sample also contained small FeO_x clusters in mesoporous channels as in the case of Fe-MCM-41-TIE.

Modification of the Fe-MCM-41-TIE and Fe-MCM-41-IMP samples with KCl changed their color from pale brown to white and increased the E_g values significantly. The KCl–Fe-MCM-41-TIE and the KCl–Fe-MCM-41-IMP samples with a K/Fe ratio of 2.0 had E_g values very close to that for the Fe-MFI sample. Moreover, as shown in Fig. 10, after KCl modification of the Fe-MCM-41-TIE sample, the intensity of the Fe K-edge XANES pre-edge peak increased distinctly, and oscillation by XANES at the high-energy region changed significantly to a pattern similar to that for the Fe-MFI or the KCl–Fe-MFI-*s* samples (curves b and d in Fig. 5). Thus we can conclude that the small FeO_x clusters in the Fe-MCM-41-TIE or the Fe-MCM-41-IMP samples were changed to highly dispersed tetrahedral iron species after modification with KCl. We speculate that this may result from a surface reaction between the FeO_x fine clusters and the KCl species.

In contrast, an inverse change occurred in the Fe-MCM-41-DHT sample after modification with KCl. A significant decrease in E_g value was observed, indicating the presence of large aggregated FeO_x particles in the KCl–Fe-MCM-41-DHT sample. Such FeO_x particles were not seen in the XRD pattern for this sample (Fig. 8), probably because the iron content was too low (<1 wt%). The XRD pattern in Fig. 7 indicates that the ordered mesoporous structure of MCM-41 was destroyed after KCl modification. Thus the interaction of KCl with the Fe-MCM-41-DHT sample probably extracted iron from the framework, forming aggregated iron oxide, and the ordered mesoporous structure collapsed at the same time. The collapse of the

mesoporous structure also caused the appearance of the crystalline KCl even at a low K/Fe ratio, as observed in Fig. 8. The segregated and poorly dispersed KCl may not be able to interact with the aggregated FeO_x particles.

It should be noted that direct modification of the Fe-MFI sample with KCl did not result in the collapse of the porous structure of MFI and the formation of FeO_x clusters. We believe that this is because the framework of the Fe-MFI zeolite is crystalline and rigid, whereas that of the Fe-MCM-41-DHT is amorphous and may be destroyed more easily.

4. Discussion

We have investigated both structural and catalytic properties of Fe-MFI and the Fe-MCM-41 samples containing iron in different locations before and after modification with KCl for the epoxidation of C_3H_6 by N_2O. Our findings suggest that the band gap energy (E_g) of the Fe–O band evaluated from the UV–vis spectrum is a simple and useful indicator for characterizing the local structure of iron. From this work and many previous studies, it is now clear that Fe-MFI and Fe-MCM-41-DHT with $E_g \geqslant 4.5$ eV contain mainly isolated (mononuclear) iron cations in the framework of MFI zeolite or MCM-41. Steam treatment of Fe-MFI at 873 K drove all or some of the framework iron cations to the extra-framework positions. Various possibilities, including mononuclear iron cations, binuclear and oligonuclear FeO_x clusters, and large FeO_x (Fe_2O_3 or Fe_3O_4) particles, have been reported as the extra-framework iron species in MFI zeolites [14–18,39–41,43–45]. The low E_g value (3.2 eV) obtained for the Fe-MFI-*s* in this work indicate the appearance of oligonuclear FeO_x clusters and possibly some Fe_2O_3 particles at the external surface of MFI. The Fe-MCM-41-TIE and the Fe-MCM-41-IMP samples both exhibited E_g values of 4.0–4.1 eV, close to the values reported by Iwamoto et al. [38] for MCM-41-encapsulated iron oxide clusters. Thus the iron species in these two samples exist mainly as small oligonuclear FeO_x clusters and are probably located in the mesoporous channels. This finding was supported by the N_2-sorption measurements and XANES and EXAFS results [31].

Without KCl modification, all of these iron-containing molecular sieves catalyzed the allylic oxidation of C_3H_6, producing acrolein and allyl alcohol as the main products. Comparisons of different catalysts revealed that C_3H_6 conversion was slightly higher over the catalysts containing mononuclear iron sites in the framework positions. In previous work [25], we suggested that the nucleophilic lattice oxygen species associated with the iron species were responsible for the allylic oxidation of C_3H_6. Our current results indicate that the framework iron in a molecular sieve can take part in oxidation by using the associated lattice oxygen. The slightly higher reactivity of the framework iron species may result from the greater dispersion of these species. The same phenomenon has been observed for the partial oxidation of CH_4 to HCHO by O_2, where Fe-MCM-41-DHT exhibited higher CH_4 conversion activity than Fe-MCM-41-TIE [32].

After modification with KCl, the structure of the Fe-MFI sample did not exhibit significant changes, and the iron remained in the framework of MFI zeolite. However, the mesoporous structure of the Fe-MCM-41-DHT sample was destroyed after the addition of KCl. The significantly low E_g value (2.8 eV) of the Fe–O band for the KCl–Fe-MCM-41-DHT sample suggests the appearance of relatively large iron oxide particles. Moreover, crystalline KCl was segregated even for the sample with a low K/Fe ratio (K/Fe = 1). In contrast, crystalline KCl was not observed for the KCl–Fe-MCM-41-TIE and the KCl–Fe-MCM-41-IMP samples even with much higher K/Fe ratios, which still had the ordered mesoporous structure. Thus KCl may be highly dispersed in the mesoporous channels in the latter two samples. More significantly, the E_g values increased to >4.5 eV after KCl modification of the Fe-MCM-41-TIE and Fe-MCM-41-IMP samples. The KCl-modified Fe-MFI-*s* samples also exhibited a significantly increased E_g. These results, together with the XANES findings, clearly suggest an enhanced dispersion of the iron species (mostly FeO_x clusters) and an altered coordination of iron from an octahedral (or square pyramidal) to a tetrahedral configuration after KCl modification. In other words, interaction or surface reaction of KCl with the FeO_x clusters in the extra-framework positions of MFI or MCM-41 led to the formation of a new type of surface tetrahedral iron structure.

Although PO became the main product after KCl modification of the Fe-MFI and the Fe-MCM-41-DHT samples, C_3H_6 conversion decreased remarkably. In contrast, KCl modification of the Fe-MFI-*s*, Fe-MCM-41-TIE, and Fe-MCM-41-IMP samples not only provided PO as the main product, but also increased the C_3H_6 conversion. The finding that the KCl–Fe-MFI-*s* sample exhibited remarkably higher TOF for PO formation than the KCl–Fe-MFI sample strongly suggests that the iron in the extra-framework position is more efficient than the framework iron. This is very different than the tendency observed for the allylic oxidation of C_3H_6 by N_2O, as discussed above. For epoxidation, an electrophilic-type oxygen species is required, and the framework iron probably is not efficient for the activation of N_2O to generate the electrophilic-type oxygen species. This also holds true for the selective oxidation of benzene to phenol. It is currently believed that iron species in the extra-framework position of MFI zeolite account for the conversion of benzene to phenol by N_2O [13–18], although the detailed structure of the active iron site remains an open question. Recent studies have revealed that framework and extra-framework Al species play important roles in obtaining high catalytic activities for benzene conversion [26–30,45]. It has been proposed that the framework Al may maintain the high-dispersion state of extra-framework iron (e.g., mononuclear iron in cationic-exchange position) [45], whereas the extra-framework Al species may interact directly with the iron species forming Fe–O–Al pair sites [26–30]. Our present results on the epoxidation of C_3H_6 by N_2O closely coincide with the finding that extra-framework iron is significantly more active than framework iron. However, in our case an alkali metal salt (i.e., KCl) is required as a modifier instead of Al. We tested the catalytic behavior of the [Fe, Al]-MFI before and after steam

treatment but obtained only a very low selectivity of PO, probably because PO can undergo easy, consecutive reactions, such as isomerization [25,46], over acidic catalysts.

The KCl–Fe-MCM-41-TIE and the KCl–Fe-MCM-41-IMP samples exhibited significantly higher TOF values for PO formation than the KCl–Fe-MFI-*s* sample. We also investigated FeO_x/Cab-O-Sil (a nonporous fumed silica) catalyst with and without KCl modification for the oxidation of C_3H_6 by N_2O and found that KCl modification shifted the main reaction route from allylic oxidation to epoxidation for this catalyst as well. However, the KCl–FeO_x/Cab-O-Sil catalyst exhibited significantly lower C_3H_6 conversion and PO selectivity than the KCl–Fe-MCM-41-TIE and the KCl–Fe-MCM-41-IMP catalysts; for example, over the KCl–FeO_x/Cab-O-Sil catalyst (Si/Fe = 100, K/Fe = 2.0), C_3H_6 conversion and PO selectivity were 1.0 and 60%, respectively, under the conditions of Table 3. We believe that the differences among these catalysts may arise because MCM-41 has much a higher surface area and ordered porous channels, which may allow the dispersion of more FeO_x clusters and KCl in homogeneous states. This is indicated by the larger E_g values for the Fe-MCM-41-TIE and the Fe-MCM-41-IMP catalysts (4.0–4.1 eV) than for the Fe-MFI-*s* and the FeO_x/Cab-O-Sil catalysts (3.0–3.2 eV). Furthermore, higher KCl content can be dispersed in the Fe-MCM-41-TIE and the Fe-MCM-41-IMP catalysts without the appearance of crystalline KCl. The finely dispersed FeO_x clusters and KCl species may have higher probabilities to react to form the active sites, that is, the highly dispersed extra-framework iron species stabilized by KCl over the KCl–Fe-MCM-41-TIE and KCl–Fe-MCM-41-IMP catalysts.

5. Conclusion

The catalysts based on Fe-MFI and Fe-MCM-41, containing either framework iron cations or extra-framework FeO_x clusters, all catalyzed the allylic oxidation of C_3H_6 by N_2O, producing acrolein and allyl alcohol as the main partial oxidation products. The samples with mononuclear iron exhibited slightly higher C_3H_6 conversion than the corresponding samples with FeO_x clusters. After modification with KCl, the main reaction route shifted to C_3H_6 epoxidation, and PO selectivities >80% could be achieved. The catalysts containing extra-framework iron species exhibited remarkably higher PO formation activity than those containing framework iron after the KCl modification. Although Fe-MFI maintained its structure, the mesoporous structure of the Fe-MCM-41-DHT sample was destroyed after the addition of KCl. In contrast, the Fe-MCM-41-TIE and the Fe-MCM-41-IMP maintained their mesoporous structures after KCl modification. The interaction of KCl with the extra-framework FeO_x clusters in the steam-treated Fe-MFI, Fe-MCM-41-TIE, and Fe-MCM-41-IMP samples increased the dispersion of iron species and generated a novel-type tetrahedral iron structure on the surface. This type of alkali metal salt-stabilized iron species may correspond to the active site for the epoxidation of C_3H_6 by N_2O.

Acknowledgments

This work was supported by the National Natural Science Foundation of China (grants. 20273054, 20021002 and 20433030), the National Basic Research Program of China (grants 2003CB615803 and 2005CB221408), the Program for New Century Excellent Talents in University of China (grant NCET-04-0602, Y.W.), and the Scientific Research Foundation for the Returned Overseas Chinese Scholars, State Education Ministry (grants to Q.Z. and Y.W.). The X-ray absorption measurements were performed with the approval of the Photon Factory (KEK-PF) Program Advisory Committee.

References

[1] M. McCoy, Chem. Eng. News 79 (43) (2001) 19.
[2] J.R. Monnier, Appl. Catal. A 221 (2001) 73, and references therein.
[3] T. Miyaji, P. Wu, T. Tatsumi, Catal. Today 71 (2001) 169.
[4] J. Lu, M. Luo, H. Lei, C. Li, J. Catal. 211 (2002) 552.
[5] J. Lu, M. Luo, H. Lei, C. Li, Appl. Catal. A 237 (2002) 11.
[6] K. Murata, Y. Liu, M. Inaba, N. Mimura, Catal. Today 91–92 (2004) 39.
[7] T. Hayashi, K. Tanaka, M. Haruta, J. Catal. 178 (1998) 566.
[8] B.S. Uphade, T. Akita, T. Nakamura, M. Haruta, J. Catal. 209 (2002) 331.
[9] A.K. Sinha, S. Seelan, S. Tsubota, M. Haruta, Angew. Chem. Int. Ed. 43 (2004) 1546.
[10] A.K. Sinha, S. Seelan, M. Okumura, T. Akita, S. Tsubota, M. Haruta, J. Phys. Chem. B 109 (2005) 3956.
[11] N. Yap, R.P. Andres, W.N. Delgass, J. Catal. 226 (2004) 156.
[12] R. Wang, X. Guo, X. Wang, J. Hao, G. Li, J. Xiu, Appl. Catal. A 261 (2004) 7.
[13] G.I. Panov, CATTECH 4 (2000) 18.
[14] G.I. Panov, A.K. Uriarte, M.A. Rodkin, V.I. Sobolev, Catal. Today 41 (1998) 365.
[15] A. Ribera, I.W.C.E. Arends, S. de Vries, J. Pérez-Ramírez, R.A. Sheldon, J. Catal. 195 (2000) 287.
[16] J. Jia, K.S. Pillai, W.M.H. Sachtler, J. Catal. 221 (2004) 119.
[17] Q. Zhu, R.M. van Teeffelen, R.A. van Santen, E.J.M. Hensen, J. Catal. 221 (2004) 575.
[18] I. Yuranov, D.A. Bulushev, A. Renken, L. Kiwi-Minsker, J. Catal. 227 (2004) 138.
[19] B.R. Wood, J.A. Reimer, A.T. Bell, M.T. Janicke, K.C. Ott, J. Catal. 225 (2004) 300.
[20] T. Yamada, K. Hashimoto, Y. Kitaichi, K. Suzuki, T. Ikeno, Chem. Lett. (2001) 268.
[21] R. Ben-Daniel, L. Weiner, R. Neumann, J. Am. Chem. Soc. 124 (2002) 8788.
[22] V. Duma, D. Hönicke, J. Catal. 191 (2000) 93.
[23] E. Ananieva, A. Reitzmann, Chem. Eng. Sci. 59 (2004) 5509.
[24] X. Wang, Q. Zhang, Q. Guo, Y. Lou, L. Yang, Y. Wang, Chem. Commun. (2004) 1396.
[25] X. Wang, Q. Zhang, S. Yang, Y. Wang, J. Phys. Chem. B 109 (2005) 23500.
[26] E.J.M. Hensen, Q. Zhu, R.A. van Santen, J. Catal. 220 (2003) 260.
[27] E.J.M. Hensen, Q. Zhu, P.-H. Liu, K.-J. Chao, R.A. van Santen, J. Catal. 226 (2004) 466.
[28] K. Sun, H. Zhang, H. Xia, Y. Liang, Y. Li, Z. Feng, P. Ying, C. Li, Chem. Commun. (2004) 2480.
[29] E.J.M. Hensen, Q. Zhu, R.A.J. Janssen, P.C.M.M. Magusin, P.J. Kooyman, R.A. van Santen, J. Catal. 233 (2005) 123.
[30] E.J.M. Hensen, Q. Zhu, R.A. van Santen, J. Catal. 233 (2005) 136.
[31] Y. Wang, Q. Zhang, T. Shishido, K. Takehira, J. Catal. 209 (2002) 186.
[32] Q. Zhang, W. Yang, X. Wang, Y. Wang, T. Shishido, K. Takehira, Microporous Mesoporous Mater. 77 (2005) 223.

[33] P. Ratnasami, R. Kumar, Catal. Today 9 (1991) 329.
[34] S. Bordiga, R. Buzzoni, F. Geobaldo, C. Lamberti, E. Giamello, A. Zecchina, G. Leofanti, G. Petrini, G. Tozzola, G. Vlaic, J. Catal. 158 (1996) 486.
[35] N.B. Figgis, Introduction of Ligand Fields, Wiley, New York, 1966.
[36] R.S. Weber, J. Catal. 151 (1995) 470.
[37] X. Gao, I.E. Wachs, J. Phys. Chem. B 104 (2000) 1261.
[38] M. Iwamoto, T. Abe, Y. Tachibana, J. Mol. Catal. A 155 (2000) 143.
[39] J. Pérez-Ramírez, G. Mul, F. Kapteijn, J.A. Moulijn, A.R. Overweg, A. Doménech, A. Ribera, I.W.C.E. Arends, J. Catal. 207 (2002) 113.
[40] A.M. Ferretti, C. Oliva, L. Forni, G. Berlier, A. Zecchina, C. Lamberti, J. Catal. 208 (2002) 83.
[41] J. Pérez-Ramírez, F. Kapteijn, J.C. Groen, A. Doménech, G. Mul, J.A. Moulijn, J. Catal. 214 (2003) 33.
[42] A.L. Roe, D.J. Schneider, R.J. Mayer, J.W. Pyrz, J. Widow, L. Que Jr., J. Am. Chem. Soc. 106 (1984) 1676.
[43] P. Martutano, L. Drozdová, A. Kogelbauer, R. Prins, J. Catal. 192 (2000) 236.
[44] K.A. Dubkov, N.S. Ovanesyan, A. Shteinman, A.E.V. Starokon, G.I. Panov, J. Catal. 207 (2002) 341.
[45] S.H. Choi, B.R. Wood, A.T. Bell, M.T. Janicke, K.C. Ott, J. Phys. Chem. B 108 (2004) 8970.
[46] J.M. Coxon, R.G.A.R. Maclagan, A. Rauk, A.J. Thorpe, D. Whalen, J. Am. Chem. Soc. 119 (1997) 4712.